Carbon Dioxide Capture

Deutsche Ausgabe: DOI: 10.1002/ange.201607055
Internationale Ausgabe: DOI: 10.1002/anie.201607055

Molecularly Designed Stabilized Asymmetric Hollow Fiber Membranes for Aggressive Natural Gas Separation

Gongping Liu[+], Nanwen Li[+],* Stephen J. Miller, Danny Kim, Shouliang Yi, Ying Labreche, and William J. Koros**

Abstract: *New rigid polyimides with bulky CF_3 groups were synthesized and engineered into high-performance hollow fiber membranes. The enhanced rotational barrier provided by properly positioned CF_3 side groups prohibited fiber transition layer collapse during cross-linking, thereby greatly improving CO_2/CH_4 separation performance compared to conventional materials for aggressive natural gas feeds.*

Membrane technology offers energy-saving and smaller footprints compared to traditional thermally driven gas amine absorption processes.[1] Recently, high-performance polymer membranes for CO_2 separation have received considerable attention and been implemented industrially.[2] Although numerous dense film polymers have been considered,[3] only a few asymmetric membranes having thin selective layers with high selectivity and permeance have actually been reported.[2c] High-pressure CO_2-induced plasticization undermines membrane separation efficiency.[4] Unfortunately most new materials are only evaluated by low-pressure, pure-gas permeation, which is far from most realistic application conditions with CO_2/CH_4 mixtures at 20–60 bar. Moreover, some feeds also contain heavier $C6^+$ hydrocarbons contaminants.[5] Cross-linking provides an effective approach to inhibit excessive swelling and segmental chain mobility in dense polymer films.[6] By optimizing the polymer structure, both permeability and selectivity can be retained or even increased in cross-linked thick films.[6c,e] While defect-free thin-skinned asymmetric membranes can be formed,[2c] structural relaxation during cross-linking to stabilize the selective layer and support morphology against aggressive feeds typically leads to significant productivity losses of two–four times.[6c,7] The loss in performance is believed to be due to significant collapse of the thin nanoporous transition layer that lies between the dense skin layer and underlying porous support, thereby causing an increase in effective skin thickness during cross-linking.[8] Clearly, overcoming the loss in productivity while stabilizing the separation performance through cross-linking is a major challenge to be overcome and is dealt with in this study.

Herein, we report a new strategy that uses a rigid copolymer structure enabled by tuning the molecular structure to inhibit nanoscale transition layer collapse, thereby providing high-performance asymmetric hollow fibers for aggressive CO_2/CH_4 feed conditions (Figure 1). Trifluoromethyl groups (CF_3) are introduced into the basic polyimide (PI) co-polymer to create a more bulky and rigid engineered molecular structure. First, (4,4′-hexafluoroisopropylidene) diphthalic anhydride (6FDA) was chosen as the monomer to form a rigid backbone with restricted torsional motion of neighboring phenyl rings due to the $-C(CF_3)_2-$ linkage, thereby providing intrinsically high perm-selectivity for CO_2 over CH_4. Common 2,4,6-trimethyl-1,3-diaminobenzene (DAM) and 3,5-diaminobenzoic acid (DABA) diamines were employed to build the basic co-polymer and promote

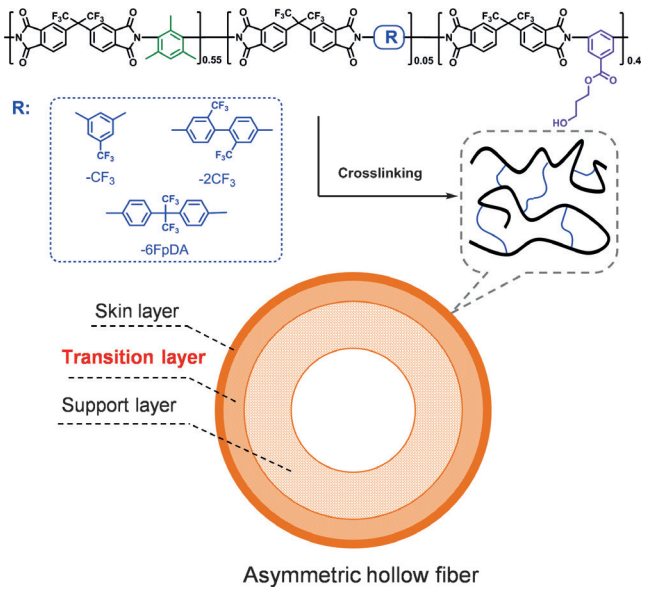

Figure 1. Structure design of cross-linkable TFM-PIs and asymmetric hollow fiber membrane.

[*] Dr. G. Liu,[+] Dr. N. Li,[+] D. Kim, Dr. S. Yi, Dr. Y. Labreche, Prof. Dr. W. J. Koros
School of Chemical & Biomolecular Engineering
Georgia Institute of Technology
Atlanta, Georgia 30332-0100 (USA)
E-mail: wjk@chbe.gatech.edu

Dr. S. J. Miller
Chevron Energy Technology Company
100 Chevron Way, Richmond, California 94802-0627 (USA)

Dr. G. Liu[+]
State Key Laboratory of Materials-Oriented Chemical Engineering
Nanjing Tech University, Nanjing 210009 (P. R. China)
E-mail: gpliu@njtech.edu.cn

Dr. N. Li[+]
State Key Laboratory of Coal Conversion, Institute of Coal Chemistry,
Chinese Academy of Sciences
Taiyuan 030001 (P. R. China)
E-mail: linanwen@sxicc.ac.cn

[+] These authors contributed equally to this work.

Supporting information for this article can be found under: http://dx.doi.org/10.1002/anie.201607055.

a high free volume and cross-linkable functionality, respectively. The additional feature explored in this work involves the incorporation of specific diamines containing CF_3 groups to further increase the rotational barrier around the backbone. The amount of such bulky diamines was limited to 5 mol% to avoid potential loss in size and shape discrimination and consequent loss in CO_2/CH_4 selectivity by excessive packing inhibition. Three types of bulky diamines providing various degrees of bulkiness and rigidities are studied: 5-(trifluoromethyl)benzene-1,3-diamine (CF_3-diamine), 2,2′-bis(trifluoromethyl)benzidine ($2CF_3$-diamine) and 4,4′-(hexafluoroisopropylidene)dianiline (6FpDA-diamine). The polyimides are designated as TFM-PI-CF_3, TFM-PI-$2CF_3$ and TFM-PI-6FpDA, respectively, corresponding to the structures in Figure 1. Synthesis details are described in the Supporting Information.

Chemical structures of the TFM-PIs were confirmed by NMR spectra of ^{19}F, ^{1}H and ^{13}C nuclei (see Figures S1–5 in the Supporting Information). For example, consider TFM-PI-CF_3 where ^{19}F shifts corresponding to Ph-CF_3 and C-$(CF_3)_2$ were observed at −62.8 ppm and −64.1 ppm, respectively[9] (Figure S1). According to the integration ratios, the molar amount of CF_3-diamine was calculated to be 5.1%, which agreed well with the stoichiometric proportion of the designed structure. ^{1}H shifts at 4.2–4.5, 3.4 and 1.6–1.7 ppm are assigned to the propanediol groups, indicating a successful monoesterification[6b] (Figures S2,3). ^{1}H NMR shifts at 10 ppm and about 11 ppm were attributed to the amide protons in DAM and DABA moieties, respectively, implying a hydrolysis of some imide rings induced by the propanediol or/and water during the monoesterification.[6d] Fortunately, the IR result in Figure S6a indicates that the opened imide rings were reclosed at the cross-linking temperature. Although 10–15% molecular weight losses were observed after the monoesterification, the TFM-PIs still exhibited high M_n values of 125000–138000 g mol^{-1} (Table S1), which is adequate for spinning good quality hollow fiber membranes.[6d] TFM-PIs can be cross-linked by simply heating in the solid state under vacuum to activate the transesterification reaction.[10] The cross-linking was inferred from the reduced O–H stretching absorption in IR spectra (Figure S6b). It was also monitored by thermogravimetric analysis (TGA). As shown in Figures S7, the weight losses of TFM-PI-CF_3 starting at 150 °C and 360 °C are related to the cross-linking induced by transesterification and decarboxylation, respectively.[10] For consistency, according to the optimization in our previous study for various monoesterified polyimides,[7c,11] we performed the cross-linking of a hollow fiber membrane at 200 °C for 2 h, and this produced a well stabilized fiber.

As mentioned above, previous hollow fiber gas permeance was remarkably reduced following cross-linking of the asymmetric hollow fiber membranes, even though the cross-linking temperature is much lower than the glass transition temperature of the polymer.[7d] We suspected that a β-transition of the polymer, related to backbone motions was promoting collapse of the nanoporous transition layer between the dense selective layer and the main microporous support (Figure 1). Dynamic mechanical thermal analysis (DMTA) was employed to investigate the β-transition of

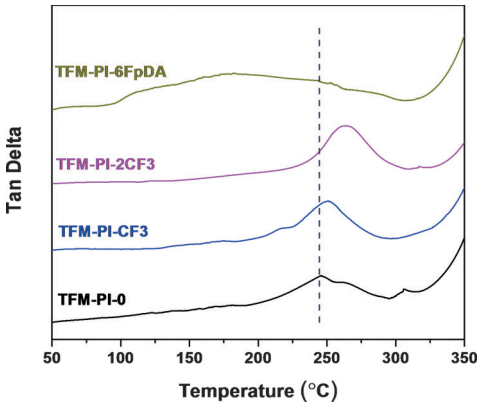

Figure 2. DMTA curves of TFM-PIs without or with CF_3-, $2CF_3$-, and 6FpDA-diamines.

TFM-PIs. As shown in Figure 2, all of the TFM-PIs showed obvious β-transitions. Introducing bulky and rigid diamines caused the TFM-PI-CF_3 to show increased peak β-transition temperature at 251 °C compared to that of the control sample without the bulky diamine (TFM-PI-0 ca. 245 °C). As expected an increase in peak β-transition temperature occurred by adding more bulkiness reflected by the higher peak β-transition temperature (ca. 264 °C) for the TFM-PI-$2CF_3$. The result suggests that, as hoped, properly placed bulky CF_3 groups due to a rigid chain architecture with CF_3 as side groups increased the rotational barrier, thereby increasing the β-transition temperature of the polymer. On the other hand, for the TFM-PI-6FpDA polymer with two bulky CF_3 groups in a more compact flexible chain, a broad and lower onset β-transition temperature was observed. Compared to the TFM-PI-0, an increased *d*-spacing was found in the TFM-PI-CF_3 and TFM-PI-$2CF_3$ films from XRD analysis (Figure S8), indicating a more packing-inhibited structure to accommodate penetrating small molecules. The bulkiness, rigidity and increased β-transition temperature considerations appear to be correlated in a complex but desirable way with gas permeation properties of the TFM-PIs films. As shown in Figure S9, the cross-linked TFM-PIs membranes containing bulky diamines showed higher CO_2 permeability compared to TFM-PI-0. The result is consistent with the anticipated higher free volume associated with addition of packing-inhibiting CF_3 side groups, which is also confirmed by the calculation of fractional free volumes by using the measured film density (Table S2). It is interesting to note that an increased CO_2/CH_4 selectivity was also observed for the TFM-PI-CF_3 and TFM-PI-$2CF_3$ membranes. The trade-off between packing inhibition due to bulkiness and rigidity of CF_3- and $2CF_3$-diamines presumably results in the desirable and unexpected increases in both permeability and selectivity. On the other hand, introduction of a flexible 6FpDA-diamine leads to an increase in CO_2 permeability, but some decrease in CO_2/CH_4 selectivity.

As discussed later, the effective as-spun dense selective layer of TFM-PI-0 asymmetric membrane was 0.15 μm, and after cross-linking, it increased to 0.36 μm as seen by SEM characterization (Figures 3c,d). It was hoped that the segmentally more rigid structure reflected by increased β-

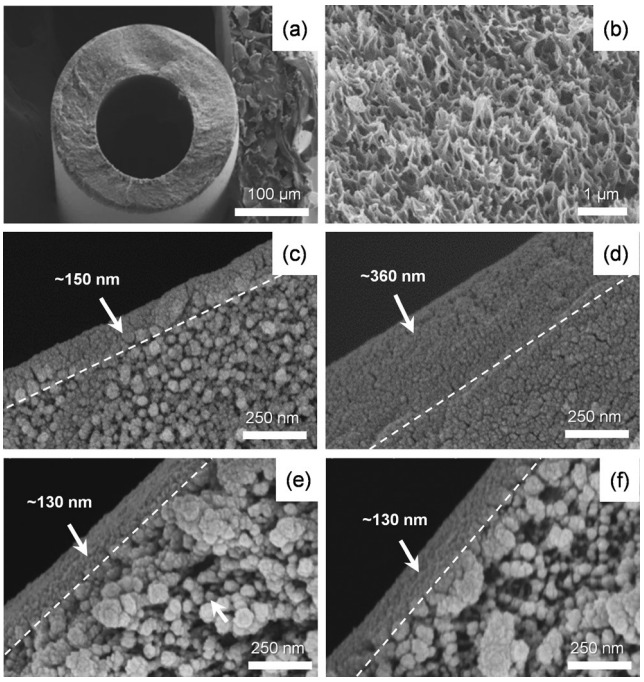

Figure 3. Cross-sectional SEM images of TFM-PI asymmetric hollow fiber membranes: a) overview; b) porous substrate layer; dense skin layer upon transition layer of TFM-PI-0 fiber c) before and d) after cross-linking; dense skin layer upon transition layer of TFM-PI-CF_3 fiber e) before and f) after cross-linking.

transition temperature for the TFM-PI-CF_3 would inhibit the transition layer collapse in asymmetric hollow fiber membranes. We fabricated TFM-PIs (TFM-PI-CF_3 and TFM-PI-0) into asymmetric hollow fiber membranes by the well-known dry-jet/wet-quench spinning method (Supporting Information) to determine this possibility. The schematic structure of the hollow fiber is displayed in Figure 1 and the actual morphologies are shown in Figures 3 and S10–12. The TFM-PI hollow fiber membranes all had regular cylindrical forms with a small outer diameter of ca. 250 μm (Figure 3 a), that provide high packing density and ability to withstand large transmembrane pressure up to ca. 55 bar. The highly porous support layer (Figures 3 b) comprises $>90\,\%$ of the total wall thickness (≈ 50 μm) of the asymmetric hollow fiber, while providing negligible transport resistance. As mentioned earlier, the structure directly beneath the dense skin layer (Figures 3 c and e), has a finer nanoporous nature, and is generally called the "transition layer". The skin layer of the TFM-PI-0 hollow fiber without CF_3-diamine becomes roughly two times thicker after cross-linking (Figures 3 c and d, S11a and b, and c and d), reflecting collapse of the finely porous structures from the transition layer. On the other hand, while undergoing the same cross-linking treatment, the 130 nm thin selective layer on the TFM-PI-CF_3 hollow fiber membrane is well preserved (Figures 3 e and f, S12a and b, and c and d). Even under ultra-high magnification, we cannot distinguish any morphology difference by cross-linking. In addition, a densification of the porous support layer observed in TFM-PI-0 fiber is also prohibited in the TFM-PI-CF_3 fiber. These results clearly indicate that introducing bulky CF_3-diamine into the TFM-PI backbone successfully inhibits nanoscale pore collapse and preserves the delicate nanostructures of asymmetric hollow fiber membrane to provide high performance properties. Gel fraction tests were also carried out to verify cross-linking stabilization of the hollow fibers.[7c] The as-spun fibers (non-cross-linked) are completely dissolved in tetrahydrofuran (THF) while cross-linked fibers only swelled and maintained their shape after 48-h soaking at 25 °C, and had a gel fraction >81 wt %. The cross-linked thin and highly solvent-resistance fibers therefore offer exciting opportunities for dealing with high-CO_2 pressure feed (e.g., natural gas separation[2c]).

To further verify the fiber property evolution, we measured 50/50 CO_2/CH_4 mixed-gas permeabilites of these TFM-PI hollow fiber membranes (Figure 4 a). The as-spun fibers (non-cross-linked) showed high CO_2 permeance (P/l_{CO_2}) of 110–115 GPU (1×10^{-6} $cm^3 cm^{-2} s^{-1} cmHg^{-1}$) and CO_2/CH_4 selectivity (α_{CO_2/CH_4}) of >32 at 35 °C and 14 bar. Interestingly, the permeance (P/l) of the asymmetric fibers is lower than the value estimated from the dense film permeability (P_{CO_2} of TFM-PI-0: 32 Barrer; TFM-PI-CF_3: 36 Barrer, Figure S9) divided by the SEM dense selective layer thickness (l, Figures 3 c,e). These results suggest that physical aging is pronounced in the asymmetric fiber of thin membrane thickness as compared to the thick dense films, which was expected based on work by Paul and co-workers.[12] As seen for the simple thick dense films, the selectivity of the TFM-PI-CF_3 fiber is higher than that of the TFM-PI-0 fiber owing to the additional rigidity of the bulky CF_3-diamine (Figure S9). After cross-linking, the CO_2/CH_4 selectivity of both TFM-PI fibers remained stable, but the cross-linked TFM-PI-0 fiber showed significantly reduced CO_2 permeance: ca. 46 GPU, 2.5 times lower than its pristine non-cross-linked permeance. The P_{CO_2} loss in the TFM-PI-0 fibers is consistent with the percentage increase in skin thickness observed in SEM (Figures 3 c,d), confirming that the cross-linking-induced nanoscale collapses undermines the permeance of the asymmetric hollow fiber. As expected, the bulky CF_3-diamine, stops nanoscale collapse (Figures 3 e,f) in the transition layer. By preventing thickening of the selective layer due to nanoscale collapse, the intrinsically high P/l_{CO_2} in the as-spun fiber is maintained in the plasticization-resistant cross-linked TFM-PI-CF_3 fiber. Moreover, we cross-linked another three batches of TFM-PI-CF_3 hollow fibers with varied as-spun skin thickness and permeance, and all the fibers held their pristine performance, like those shown in Figure S13. Besides outstanding reproducibility, these results suggest that the excellent prevention of nanoscale transition layer collapse may be feasible for even thinner skinned fibers to achieve even higher permeance.

The applicability of the cross-linked TFM-PI-CF_3 hollow fibers was demonstrated further in aggressive high-pressure mixed gas tests with 50/50 CO_2/CH_4 mixtures. Typical results are given in Figure 4 b. Neither permeance upswing nor selectivity decline is found, even as the feed pressure goes up to 55 bar. The slight permeance drop at high pressure is due to the well-known dual mode sorption effect.[4] The results clearly prove the absence of CO_2 plasticization in the cross-linked TFM-PI-CF_3 fiber. To pursue additional realistic

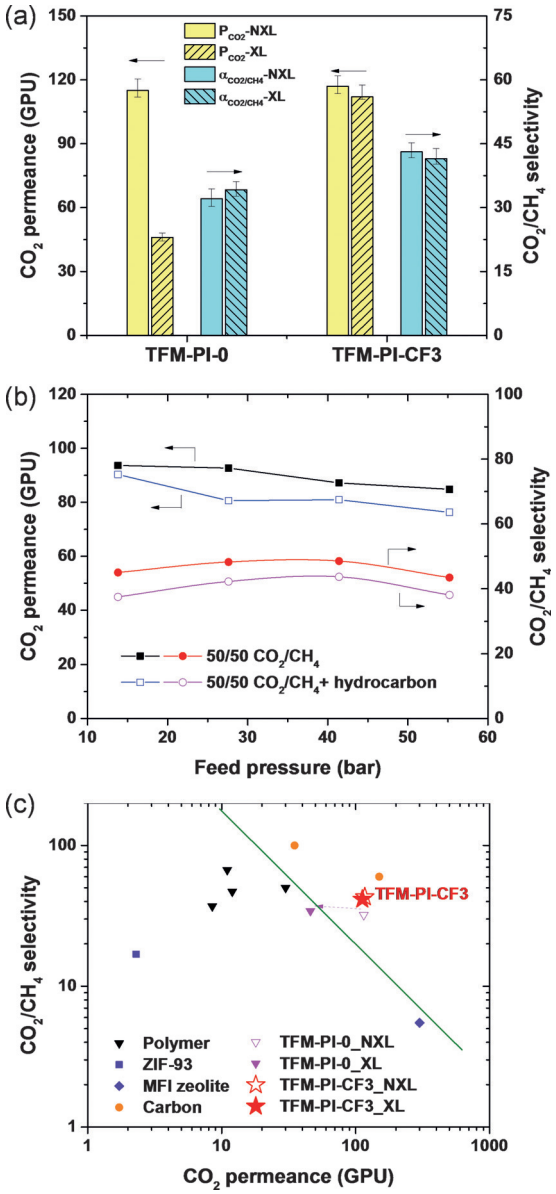

Figure 4. Gas separation performance of hollow fiber membranes: a) comparison between TFM-PI-0 and TFM-PI-CF_3 hollow fiber membrane before and after cross-linking, non-cross-linked (NXL), cross-linked (XL), feed conditions: 50:50 CO_2/CH_4 mixtures, 14 bar, 35 °C; b) cross-linked TFM-PI-CF_3 hollow fiber membrane tested under feed pressure up to 55 bar with or without hydrocarbon in 50:50 CO_2/CH_4 mixtures at 35 °C; c) comparison of CO_2 permeance and CO_2/CH_4 selectivity reported for hollow fiber membranes under mixed-gas permeation, more details are listed in Table S3. The green eye-guiding line is only used to indicate the general "trade-off" between permeance and selectivity in hollow fiber membranes.

natural gas application,[5] we also explored effects of 300 ppm heptane as model hydrocarbon in the feed to continue the high-pressure test. The cross-linked TFM-PI-CF_3 fiber still exhibited excellent plasticization resistance and high performance under these extremely challenging feed conditions. The slightly lower permeance and selectivity presumably reflects free volumes filling by the heptane.[13] This negative effect on permeance is more significant with the presence of toluene, with up to 29% loss of permeance for the cross-linked TFM-PI-CF_3 fiber in the feed of 50/50 CO_2/CH_4 mixtures containing 250 ppm heptane and 250 ppm toluene at 35 °C and 55 bar. Moreover, even in this very aggressive feed, we did not observe the plasticization, and meanwhile α_{CO_2/CH_4} remained above 30, while the non-cross-linked TFM-PI-CF_3 fiber showed a typical plasticization behavior with permeance upswing at higher feed pressure (Figure S14). Impressively, we found the non-cross-linked fiber could maintain $\alpha_{CO_2/CH_4} > 35$ even though at the highest pressure of 55 bar, despite minor plasticization being apparent. These results suggest that the extra benefits given by the enhanced chain rigidity may allow applying the non-cross-linked TFM-PI-CF_3 fiber in some moderate-pressure CO_2 separation.

As mentioned earlier, advantages in higher packing density and durability under high pressures make the fiber and even small tubes attractive and have promoted some studies of various materials beyond flat dense films in such formats that can be scaled up. Polymers, zeolite, metal–organic frameworks or carbon molecular sieves, have been considered in this regards for CO_2/CH_4 separation. Figure 4c and Table S3 provide comparison of CO_2 permeance and CO_2/CH_4 selectivity including the state-of-the-art hollow fibers discussed here and the earlier cases of highly permeable hollow fibers made by conventional polyimides that lost two–five times in permeance after cross-linking.[7a,b,d] The newly designed TFM-PI-CF_3 structure, to our best knowledge, represents the first successful maintenance of high permeance and intrinsic selectivity in a cross-linked hollow fiber with excellent CO_2/CH_4 separation performance. Moreover, this performance is maintained under >6000 minutes of long-term operation with a 50:50 CO_2/CH_4 mixture at 55 bar (Figure S15). Compared with flat asymmetric cellulose acetate membranes[14] for natural gas processing plants,[2c] we achieved a 2–25 times improved permeance and a two–three times improved selectivity. In addition, the ultra-permeable TFM-PI-CF_3 hollow fiber, after 240 days of aging under air storage at room temperature (Figure S16), only lost 14% CO_2 permeance, which is three times less than the traditional PI hollow fibers,[13] and meanwhile gained 8% CO_2/CH_4 selectivity (P/l_{CO_2} ca. 83 GPU, α_{CO_2/CH_4} ca. 50). This outstanding anti-aging property of the asymmetric fiber is again attributed to the bulky and rigid TFM-PI-CF_3 structure.

In conclusion, new CF_3-containing polyimides (TFM-PIs) were synthesized and translated into high-performance cross-linkable asymmetric hollow fiber membranes. The introduction of bulky CF_3-diamine hindered segmental motion, as reflected by increased β-transition temperature of TFM-PI polymer. This hindrance in segmental motion stabilized the nanoscale transition layer morphology in asymmetric hollow fiber membranes during thermal cross-linking. The cross-linked TFM-PI-CF_3 hollow fiber exhibited extraordinary high and stable separation performance for high-pressure and aggressive CO_2/CH_4 mixtures. Optimization of molecular composition and polymer spinning could further advance the fiber performance. The polymer design strategy presented here provides a new platform of developing high-performance hollow fiber membranes for realistic high-pressure CO_2 separation. Additional work is underway to also explore

hollow fibers based on the TFM-PI-2CF_3; however, this is clearly very time-consuming and will be reported in the future.

Acknowledgements

This work was financially supported by Chevron Energy Technology Company and DOE Basic Energy Sciences.

Keywords: carbon dioxide capture · cross-linking · hollow fibers · membranes · natural gas

How to cite: *Angew. Chem. Int. Ed.* **2016**, *55*, 13754–13758
Angew. Chem. **2016**, *128*, 13958–13962

[1] a) W. J. Koros, G. K. Fleming, *J. Membr. Sci.* **1993**, *83*, 1–80; b) W. J. Koros, *AIChE J.* **2004**, *50*, 2326–2334; c) D. L. Gin, R. D. Noble, *Science* **2011**, *332*, 674–676.

[2] a) P. Bernardo, E. Drioli, G. Golemme, *Ind. Eng. Chem. Res.* **2009**, *48*, 4638–4663; b) W. J. Koros, R. P. Lively, *AIChE J.* **2012**, *58*, 2624–2633; c) R. W. Baker, B. T. Low, *Macromolecules* **2014**, *47*, 6999–7013.

[3] a) H. Lin, E. Van Wagner, B. D. Freeman, L. G. Toy, R. P. Gupta, *Science* **2006**, *311*, 639–642; b) H. B. Park, C. H. Jung, Y. M. Lee, A. J. Hill, S. J. Pas, S. T. Mudie, E. Van Wagner, B. D. Freeman, D. J. Cookson, *Science* **2007**, *318*, 254–258; c) M. Carta, R. Malpass-Evans, M. Croad, Y. Rogan, J. C. Jansen, P. Bernardo, F. Bazzarelli, N. B. McKeown, *Science* **2013**, *339*, 303–307; d) T.-H. Bae, J. S. Lee, W. Qiu, W. J. Koros, C. W. Jones, S. Nair, *Angew. Chem. Int. Ed.* **2010**, *49*, 9863–9866; *Angew. Chem.* **2010**, *122*, 10059–10062; e) J. Shen, G. Liu, K. Huang, W. Jin, K.-R. Lee, N. Xu, *Angew. Chem. Int. Ed.* **2015**, *54*, 578–582; *Angew. Chem.* **2015**, *127*, 588–592; f) S. Wang, X. Li, H. Wu, Z. Tian, Q. Xin, G. He, D. Peng, S. Chen, Y. Yin, Z. Jiang, M. D. Guiver, *Energy Environ. Sci.* **2016**, *9*, 1863–1890.

[4] J. D. Wind, S. M. Sirard, D. R. Paul, P. F. Green, K. P. Johnston, W. J. Koros, *Macromolecules* **2003**, *36*, 6433–6441.

[5] A. A. Olajire, *Energy* **2010**, *35*, 2610–2628.

[6] a) C. Staudt-Bickel, W. J. Koros, *J. Membr. Sci.* **1999**, *155*, 145–154; b) J. D. Wind, C. Staudt-Bickel, D. R. Paul, W. J. Koros, *Macromolecules* **2003**, *36*, 1882–1888; c) A. M. W. Hillock, W. J. Koros, *Macromolecules* **2007**, *40*, 583–587; d) I. C. Omole, S. J. Miller, W. J. Koros, *Macromolecules* **2008**, *41*, 6367–6375; e) W. Qiu, C.-C. Chen, L. Xu, L. Cui, D. R. Paul, W. J. Koros, *Macromolecules* **2011**, *44*, 6046–6056; f) Q. Song, S. Cao, R. H. Pritchard, B. Ghalei, S. A. Al-Muhtaseb, E. M. Terentjev, A. K. Cheetham, E. Sivaniah, *Nat. Commun.* **2014**, *5*, 4813; g) K. Vanherck, G. Koeckelberghs, I. F. J. Vankelecom, *Prog. Polym. Sci.* **2013**, *38*, 874–896.

[7] a) C. Cao, T.-S. Chung, Y. Liu, R. Wang, K. P. Pramoda, *J. Membr. Sci.* **2003**, *216*, 257–268; b) P. S. Tin, T. S. Chung, Y. Liu, R. Wang, S. L. Liu, K. P. Pramoda, *J. Membr. Sci.* **2003**, *225*, 77–90; c) D. W. Wallace, J. Williams, C. Staudt-Bickel, W. J. Koros, *Polymer* **2006**, *47*, 1207–1216; d) I. C. Omole, R. T. Adams, S. J. Miller, W. J. Koros, *Ind. Eng. Chem. Res.* **2010**, *49*, 4887–4896.

[8] J. J. Krol, M. Boerrigter, G. H. Koops, *J. Membr. Sci.* **2001**, *184*, 275–286.

[9] A. Y. Vainer, K. M. Dyumaev, A. M. Kovalenko, A. N. Vintin, Y. I. Maze, Y. A. Mendeleva, *Dokl. Phys. Chem.* **2009**, *427*, 159–162.

[10] W. Qiu, C.-C. Chen, M. R. Kincer, W. J. Koros, *Polymer* **2011**, *52*, 4073–4082.

[11] C. Ma, W. J. Koros, *J. Membr. Sci.* **2013**, *428*, 251–259.

[12] M. S. McCaig, D. R. Paul, J. W. Barlow, *Polymer* **2000**, *41*, 639–648.

[13] C. Ma, W. J. Koros, *J. Membr. Sci.* **2014**, *451*, 1–9.

[14] a) T. Visser, N. Masetto, M. Wessling, *J. Membr. Sci.* **2007**, *306*, 16–28; b) R. W. Baker, *Ind. Eng. Chem. Res.* **2002**, *41*, 1393–1411.

Received: July 20, 2016
Revised: September 3, 2016
Published online: October 4, 2016

